

Active View Planning for Visual SLAM in Outdoor Environments Based on Continuous Information Modeling

Zhihao Wang, Haoyao Chen*, *Member, IEEE*, Shiwu Zhang, *Member, IEEE*, Yunjiang Lou, *Senior Member, IEEE*

Abstract—The visual simultaneous localization and mapping (vSLAM) is widely used in satellite-denied and open field environments for ground and surface robots. However, due to the frequent perception failures derived from featureless areas or the swing of robot view direction on rough terrains, the accuracy and robustness of vSLAM are still to be enhanced. The study develops a novel view planning approach of actively perceiving areas with maximal information to address the mentioned problem; a gimbal camera is used as the main sensor. Firstly, a map representation based on feature distribution-weighted Fisher information is proposed to completely and effectively represent environmental information richness. With the map representation, a continuous environmental information model is further established to convert the discrete information space into a continuous one for numerical optimization in real-time. Subsequently, the receding horizon optimization is utilized to obtain the optimal informative viewpoints with simultaneously considering the robotic perception, exploration and motion cost based on the continuous environmental model. Finally, several simulations and outdoor experiments are performed to verify the improvement of localization robustness and accuracy by the proposed approach. We release our implementation as an open-source¹ package for the community.

Index Terms—Localization uncertainty representation, continuous information modeling, active view planning, receding horizon optimization.

I. INTRODUCTION

Visual SLAM is widely used in outdoor and field environments for environmental monitoring, resource exploration and lakeshore inspection since the solution is of low cost and rich perceptual information [1], [2]. However, the outdoor environments, like rough terrains and featureless water surface or ground, introduce difficulties for commonly used vSLAM algorithms [3] to achieve robust performance. For example, when the surface robot is floating along the lakeshore for inspection or cleaning, the featureless water surface will occupy large field-of-view (FOV); when the ground robot is moving uphill, the perception system on the robot may tilt with the body to look towards the sky. These conditions easily lead to lost features and failure of localization. The inertial measurement unit (IMU) measurements and vision are fused to deal with feature loss in featureless and dynamic environments [4]. However, robot pose tracking often fails when working for a long time in the complex environments due to the loss of

visual tracking [5]. Likewise, the large FOV cameras which can observe more features [6] are utilized for robust tracking in featureless scene; however the loss of angular resolution for higher FOVs is drastically amplified by the higher depth range in outdoor environments [7], leading to the worse tracking performance than the perspective camera.

Animals with necks can turn their view flexibly to areas of interest. Similarly, actively controlling sensors like a camera to look at the places with rich features will benefit robotic navigation performance. Besides, the robotic trajectory may be defined by the operator in remote monitoring and operating applications like lakeshore inspection. Thus, the view planning problem - where to look and how to look under the predefined trajectory - is essential to improve the estimation accuracy [8]. To address the problem, this paper utilizes a gimbal camera which can turn the camera toward the best view with minimal estimation uncertainty. Note that the whole-body planning of camera view and robotic trajectory together is another research topic and is out of the research scope of this paper.

Generally, for the active visual SLAM, three challenging issues need to be considered [9], namely, how to represent the robotic state estimation uncertainty with respect to the camera view, how to evaluate the performance of the candidate views to consider the trade-off of viewing new places (i.e., exploration) and reducing the estimation uncertainty by re-viewing known feature points (i.e., exploitation), and how to select the next best view in all candidate views in real-time.

The estimation uncertainty depends on many factors like texture, illumination [10], and dynamic or static environmental objects. Various indicators like feature numbers [11], and Fisher information [12], [13] are generally used for evaluating the estimation uncertainty. The feature numbers-based solution utilizes the numbers of feature points in the view to represent the estimation uncertainty. However, it is difficult to quantify the uncertainty of each feature point. The Fisher information-based solution is able to quantify the uncertainty meaningfully. For the information computation, the existing approaches based on feature points [12] needs to calculate the Jacobian matrix of each feature, resulting in computation efficiency suffering. The localization information is summarized into voxels by using Fisher information field to accelerate the computation for online planning, but the building time of the field is still higher due to the iteration of each feature [13]. Voxelization [14] can be used to accelerate the map building process by downsampling the feature points, but the voxelization concentrates on the occupancy of each voxel and neglects point distribution in the voxel. This neglect results in the ambiguity of the estimation uncertainty representation when calculating Fisher information with voxels. The ambiguity

This work was supported in part by the National Natural Science Foundation of China under Grant U1713206. (Corresponding author: Haoyao Chen.)

Z.H. Wang, H.Y. Chen*, Y.J. Lou are with the School of Mechanical Engineering and Automation, Harbin Institute of Technology Shenzhen, P.R. China, e-mail: hychen5@hit.edu.cn.

S.W. Zhang is with the Department of Precision Machinery and Precision Instrumentation, University of Science and Technology of China (swzhang@ustc.edu.cn)

¹Code is available at <https://github.com/HITSZ-NRSL/IGLOV.git>

is described in Section III in detail. Therefore, the accurate and efficient representation of environmental estimation uncertainty for online mapping and planning remains challenging.

Besides the information representation, the evaluation of candidate views for robotic exploration/exploitation is also an essential problem for active SLAM. For exploration, many researchers utilize lasers or cameras to detect geometric frontiers or calculate information gain to plan the sensor movement [15]; the purpose is to completely explore the unknown environments as soon as possible. For exploitation, some approaches plan a feature-rich trajectory to minimize the state estimation uncertainty with a camera fixed on a quad-rotor [16] or a gimbal camera on a mobile robot [17]. However, due to the greedy consideration of the minimal localization uncertainty, the existing methods [16], [17] suffer from continuously revisiting known areas without exploring unknown areas. This leads to the degeneration [17] or local minimum problem [9] of planning, especially for the view planning in unknown environments. Some approaches have been developed by utilizing a mode switching mechanism [8], [9], [18] to address the exploration-exploitation dilemma. A solution presented in [8] involved switching the exploitation mode to the exploration mode when sufficient landmarks are successfully detected. Different weights were assigned to the modes in [9], [18], and balancing the SLAM uncertainty reduction and area coverage task performed well. By contrast, this study utilizes motion consistency [19] as an exploration indicator to deal with the degeneration problem of view planning. The motion consistency produces attractive force to keep the next best view being consistent with the motion direction. Subsequently, the evaluation of candidate views considers both the exploitation of information and the exploration indicator in an objective function; this makes it possible to solve the exploration-exploitation dilemma with continuous planning.

Based on the evaluation of candidate views, sample-based methods, e.g., RRT* [17], or Dynamic movement primitive [20] were developed to select the best view with maximal utility. The methods suffer from discontinuous motion due to the discrete sampling. Some researchers [21], [22] realized continuous-space planning by maximizing the utility of candidate states. However, the utility function of informative path planning is always high-dimensional, nonlinear, and non-convex, which makes solving the optimization problem of maximizing the utility difficult. The evolutionary algorithm is used to solve the complex optimization problem [21], but it is time-consuming. The gradient descent is an efficient optimization technology but hard to derive an analytic expression of the complex utility function's gradient [22].

The paper aims to develop a novel approach by actively and smoothly controlling a gimbal camera equipped on the robot to realize robust and accurate SLAM in unknown outdoor environments. The three challenging issues mentioned above are solved efficiently in the proposed approach. The contributions of the paper are three-fold.

First, a novel map representation based on feature distribution-weighted Fisher information is proposed to store the localization uncertainty of environments. This new information map overcomes the ambiguity of the localization un-

certainty representation of the traditional voxelization method. Our method makes the environmental information representation more accurate and efficient for active perception and further helps realize online information mapping and motion planning.

Second, a continuous information modeling method is proposed to map the environmental information, like localization uncertainty around the robot, into multiple polynomial functions. The polynomial functions provide analytic derivatives for the environmental information with respect to the action space, and therefore makes the informative planning problem be solved efficiently by numerical optimization with lightweight time-consuming.

Third, an information gradient-based local view (IGLOV) planner is proposed to plan the optimal camera views in real-time for obtaining maximal environmental information. The planner realizes active view planning by considering the estimation uncertainty, exploration for avoiding degeneration and motion smoothness constraints simultaneously. The experiments illustrate that our approach outperforms the state of the art.

II. SYSTEM OVERVIEW

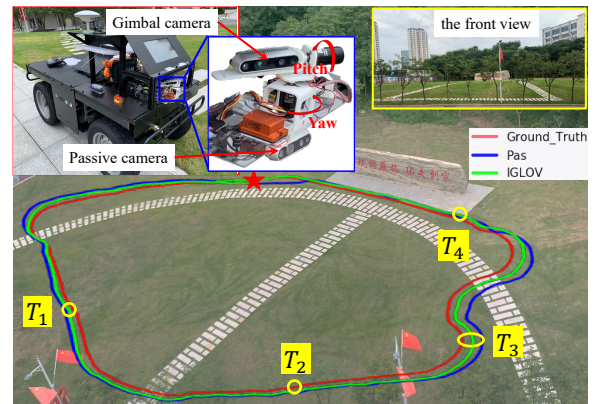


Fig. 1. Illustration of active view planning of a gimbal camera for visual SLAM in an outdoor environment.

This work considers a ground or surface robot traveling along predefined trajectories in unknown outdoor environments, as illustrated in Fig. 1. A camera is equipped on the robot through a two-axis gimbal. To guarantee the robustness of trajectory tracking, a robust visual SLAM is required by automatically changing the camera perception direction to achieve stable state estimation. Therefore, the problem to be addressed in this work is formulated as

$$\begin{aligned} \mathbf{u}^* &:= \arg \max_{\mathbf{u}} f(\xi^{\text{wc}}, \mathcal{M}, \mathbf{u}) \\ \text{s.t. } &h(\xi^{\text{wc}}, \mathbf{u}) \leq 0 \end{aligned} \quad (1)$$

where $f(\cdot)$ denotes an objective function to be designed that quantifies the estimation accuracy of the camera pose ξ^{wc} ; \mathcal{M} denotes the estimated map; \mathbf{u} including yaw and pitch control commands denotes the control vector of the gimbal to be optimized; \mathbf{u}^* is the optimal control vector of \mathbf{u} ; $h(\cdot)$ represents the constraints for the gimbal camera; $\xi^{\text{wc}} = [\chi^{\text{wc}}, \phi^{\text{wc}}]^T \in \mathbb{R}^6$ denotes the camera pose with respect

to the world frame, where $\chi^{\text{wc}} \in \mathbb{R}^3$ and $\phi^{\text{wc}} \in \mathbb{R}^3$ denote the translation and rotation, respectively.

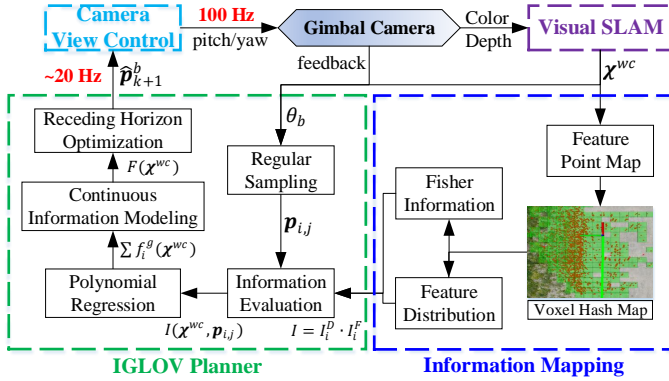


Fig. 2. Framework of the proposed active visual SLAM approach.

Figure 2 illustrates a framework of active visual SLAM by integrating the proposed solutions of information mapping, continuous environmental modeling and camera view planning. The camera poses together with the feature point map are obtained using the common visual SLAM. The information mapping process lies in evaluating the information richness of the environment; to achieve the objective, a mapping method that includes both Fisher information and feature distribution information is proposed. We use the Fisher information to evaluate the estimation uncertainty stored in the voxel like [13], and use feature distribution information to evaluate feature number and distribution in the voxel. Based on the above information mapping, the camera view planning algorithm is then developed to obtain the camera's best view direction; the direction is represented by the means of a view-landing-point. The algorithm consists of four steps, including the generation of sample points, the evaluation of information gain, polynomial regression, and receding horizon optimization. Finally, the best view-landing-point obtained from the algorithm is sent to the bottom tracking controller of the gimbal.

III. ENVIRONMENTAL INFORMATION MAPPING

The information richness of the surrounding environment should be evaluated to guide the camera view planning. The voxelization is used to efficiently represent the information richness of the environment by downsampling the feature point cloud. However, the representation with voxelization raises a new problem in active perception. The information calculated from the voxel map represents the localization uncertainty of each voxel but neglects the effect of the feature number in the voxel and the feature distribution around the voxel on the localization uncertainty. Especially for the feature-based vSLAM, the feature number and their distribution uniformity directly affect the tracking accuracy [4]. Specifically, the neglect of feature distribution results in feature-dense areas that have the same information as the feature-sparse areas; however, feature-dense areas actually contain more features for tracking than feature-sparse areas. This problem is called as the ambiguity in the representation of estimation uncertainty brought by voxelization. To deal with the ambiguity problem, the feature distribution information, including the feature

number in the voxel and the feature distribution around the voxel, is integrated with the Fisher information of a voxel. The integration of the two kinds of information is realized by a new map representation method to evaluate the information richness of the environment.

A. Calculation of Fisher information

The Fisher information matrix (FIM) indicates the *Cramér – Rao* lower bound, the smallest covariance of an unbiased estimator [23]. Therefore, the Fisher information matrix is usually used to represent the estimation uncertainty in many robotic applications like feature selection [24].

As our approach focuses on the view planning based on the known feature point maps obtained from SLAM, the uncertainty of camera pose estimation is evaluated from the perspective of observation uncertainty to decide the next best view. The observation uncertainty is evaluated by the Fisher information that carry about estimating the camera pose ξ^{wc} . The observation z_i of p_i^{w} at the camera pose ξ^{wc} is modeled as

$$z_i = g(\xi^{\text{wc}}, p_i^{\text{w}}) + \omega \quad (2)$$

where $g(\cdot)$ is derived from the camera's measurement model; here the bearing vector model is implemented as the measurement model [25] and is defined as

$$g(\xi^{\text{wc}}, p_i^{\text{w}}) = p_i^{\text{c}} / \|p_i^{\text{c}}\|_2, p_i^{\text{c}} = (\exp(\xi^{\text{wc}} \wedge))^T p_i^{\text{w}}. \quad (3)$$

where p_i^{w} and p_i^{c} denotes the center position of the i th voxel V_i in the world coordinate frame and the camera coordinate frame, respectively. $i = 0, 1, \dots, M$ and M is the number of occupied voxels of the voxel map \mathcal{M} ; ω denotes white noise with covariance \mathbf{Q} . Then, the Fisher information matrix $I_i \in \mathbb{R}^{6 \times 6}$ evaluates the estimation uncertainty derived from the observation of p_i^{w} at ξ^{wc} , and is defined as:

$$I_i = J_g^T Q^{-1} J_g \quad (4)$$

where $J_g = \partial g / \partial \xi^{\text{wc}}$ denotes the Jacobian of the observation function $g(\cdot)$ with respect to ξ^{wc} . For detailed deduction, please refer to [26]. Because $\{I_0, \dots, I_M\}$ is a series of matrices, the memory usage increases rapidly with the environmental exploring. A common way to evaluate voxels in terms of estimation accuracy is based on the theory of optimal experimental design (TOED) [27]. TOED utilizes the T-opt optimality criterion, i.e., the trace of the FIM, to convert the matrix to a scalar metric for reducing memory usage. Moreover, it has been proved that the Fisher information matrix without the visibility constraint is rotation-invariant [25]; that means the FIM only relates to the camera position χ^{wc} , and not concerned with the camera rotation ϕ^{wc} . Therefore, we finally define the Fisher information metric I_i^F as

$$I_i^F(\chi^{\text{wc}}, p_i^{\text{w}}) = \text{trace}(I_i) \quad (5)$$

where $I_i^F(\chi^{\text{wc}}, p_i^{\text{w}})$ represents the estimation uncertainty of χ^{wc} when observing V_i at χ^{wc} .

B. Calculation of distribution-weighted Fisher information

The uniformity of feature distribution affects the tracking accuracy in the feature-based SLAMs. The statistics of features in the neighbor voxel set S_{ne} , which consisted of the 27 neighbor voxels around V_i , are used to formulate the uniformity of

feature distribution. Specifically, the mean and the standard deviation of the feature number in S_{ne} are defined as

$$\mu_i = \frac{1}{N_{ne}} \sum_{k=1}^{N_{ne}} N_k^D \quad (6)$$

$$\sigma_i = \sqrt{\frac{\sum_{k=1}^{N_{ne}} (N_k^D - \mu_i)^2}{N_{ne}}} \quad (7)$$

where N_{ne} is the element number in S_{ne} ; N_k^D denotes the feature number within the k -th neighbor voxel V_k in S_{ne} . The uniformity I_i^D of feature distribution around V_i is defined as

$$I_i^D = \mu_i \cdot (1 + e^{-\sigma_i}). \quad (8)$$

Because the calculation of Fisher information is based on the discrete voxels, which neglects the feature number and distribution around the voxel, we complement the Fisher information with the feature distribution of each voxel for accurate representation. I_i^F concentrates on the estimation uncertainty of the camera pose in a voxel. While I_i^D focuses on the local feature distribution around the voxel, which explicitly represents the localization uncertainty from the perspective of feature matching and tracking. Then the information in (5) and (8) are fused as

$$I(\chi^{\text{wc}}, \mathbf{p}_i^{\text{w}}) = I_i^D \cdot I_i^F(\chi^{\text{wc}}, \mathbf{p}_i^{\text{w}}) \quad (9)$$

where $I(\chi^{\text{wc}}, \mathbf{p}_i^{\text{w}})$ denotes the distribution-weighted Fisher information of χ^{wc} when observing V_i at χ^{wc} .

Based on (9), the distribution-weighted Fisher information by considering both the Fisher information and the feature distribution is able to correctly quantify the estimation uncertainty of camera poses. It provides the essential information metric for the camera view planning module in the following section.

IV. CAMERA VIEW PLANNING

Literature [18] has shown that the known areas of the map have more known features for tracking and contribute to low uncertainty, whereas unknown areas generally have fewer features and lead to high uncertainty. Therefore, the maximum information-based solution allows the robot to only revisit the known areas for robust localization. This condition may lead to the degeneration of navigation, especially for the active camera view planning in unknown environments. To address the problem, we develop a novel information gradient-based local view (IGLOV) planner to actively minimize localization uncertainty while considering the degeneration simultaneously. The IGLOV planner contains four main parts, i.e., generating sample points, evaluating information gain, conducting polynomial regression, and receding horizon optimization.

As the gimbal camera has only two degrees of freedom, solving the inverse kinematic is convenient. Furthermore, its view planning in task space can benefit the motion prediction and handling of environmental perception. Therefore, the planner optimizes the view-landing-points in task space; the view-landing-point means the intersection of the terrain surface and the camera optical axis. Followed by the gimbal's inverse kinematics, the view-landing-point will be transformed into desired gimbal rotation angles. Besides, "point" is used to

denote "view-landing-point" for simplification in the rest of the paper.

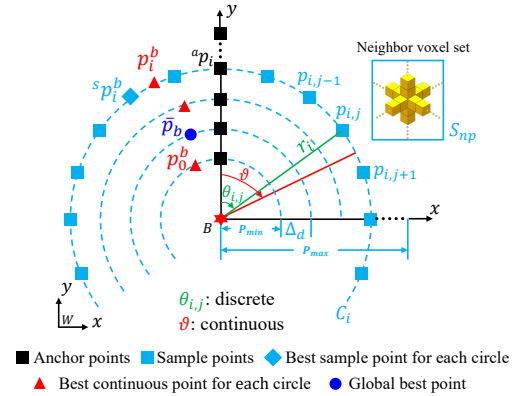


Fig. 3. View-landing-point sampling process in the IGLOV planner.

A. Generation of sample points

As shown in Fig.3, the red star denotes the current pose of the robot, and frames W and B represent the world and the robot base coordinate frames, respectively. The y-axis of $X_B - O_B - Y_B$ is along the robot's moving direction. The anchor points are firstly generated along the y-axis. Moreover, each anchor point $^a p_i$ corresponds to a sample circle C_i for generating the sample points. Sample points are uniformly generated from $^a p_i$ to both sides along the sample circle C_i with radius r_i and angle interval $\Delta\theta$. The j th sample point on i th sampling circle C_i is denoted as $\mathbf{p}_{i,j}$, and its coordinates w.r.t. the world frame is given as

$$\mathbf{p}_{i,j} = \chi^{\text{wc}} + [r_i * \sin(\theta_{i,j} + \theta_b), r_i * \cos(\theta_{i,j} + \theta_b), 0]^T \quad (10)$$

where $r_i = P_{min} + i * \Delta_d$, $i = 0, 1, \dots, N_{AP}$, P_{min} is the minimal range for the anchor points, Δ_d is the distance interval between two neighboring anchor points along the radial direction, N_{AP} is the number of anchor points; $\theta_{i,j} = k * \Delta\theta$, $k = -N_{SP}/2, \dots, -1, 0, 1, \dots, N_{SP}/2$, $j = 0, 1, \dots, N_{SP}$, N_{SP} is the number of sample points along C_i , $\theta_{i,j}$ is the angle between $\mathbf{p}_{i,j}$ and $^a p_i$, and $\Delta\theta$ is the angle interval between two neighboring sample points (e.g., $\mathbf{p}_{i,j-1}$ and $\mathbf{p}_{i,j}$); θ_b is the yaw angle of the robot base calculated from ϕ^{wb} , and ϕ^{wb} is the orientation of the robot base.

B. Evaluation of information gain

To evaluate the information gain of the sample points, a function is constructed with considering both the localization uncertainty and degeneration. The localization uncertainty is quantified by the information defined in (9). Further, the consistency between the view direction of the gimbal camera and the motion direction of the robot base is considered to deal with the degeneration. Thus, the information gain function of the sample point $\mathbf{p}_{i,j}$ is defined as

$$g_{i,j} = I(\chi^{\text{wc}}, \mathbf{p}_{i,j}) - \lambda_d \cdot |\theta_{i,j}| \quad (11)$$

where $I(\chi^{\text{wc}}, \mathbf{p}_{i,j})$ denotes the information of the voxel $\mathbf{p}_{i,j}$ calculated by (9); $|\theta_{i,j}|$ denotes the absolute value of $\theta_{i,j}$; $\lambda_d := I(\chi^{\text{wc}}, \mathbf{p}_{i,j})/\pi$ is a dynamic weight coefficient for balancing the two terms into the same magnitude. The term $|\theta_{i,j}|$ represents the consistency between the view direction corresponding to the sample point $\mathbf{p}_{i,j}$ and the robotic motion

direction, as demonstrated in Fig.3. Thus, it penalizes the sample points deviating from the motion direction.

Equation (11) calculates the information gain of the single view-landing-point $\mathbf{p}_{i,j}$; however, it raises the problem that the information of a single point cannot wholly represent the information within the camera's FOV. To this end, we consider the information around the sample point $\mathbf{p}_{i,j}$ by involving the neighboring voxel set S_{np} within a predefined distance threshold d_n . Through the addition of S_{np} into the information gain function, the planner takes the 3D environmental information into consideration even though with a 2D sampling method. Finally, the information gain function (11) is rewritten as

$$g_{i,j} = \sum_{\mathbf{p}_{np} \in S_{np}} I(\chi^{\text{wc}}, \mathbf{p}_{np}) - \lambda_d \cdot |\theta_{i,j}| \quad (12)$$

where \mathbf{p}_{np} denotes an element in the set S_{np} .

C. Polynomial regression for continuous information gain

The camera view planning is modeled as an optimization problem by evaluating the points in the task space. However, the information gain function defined in (12) is discrete. For the convenience of numerical optimization, the function to be optimized must be continuous and differentiable. To address the problem, we apply the methodology of polynomial regression to approximate a continuous and differentiable function about the environmental information. Compared with Gaussian process regression and other surface fitting methods, the polynomial regression for each curve is efficient, with the mathematics expression being differentiable. After the polynomial regression, the best point of the local environment can be obtained by searching the point with the maximal information gain in the multiple polynomial curves. Besides, the optimal result based on multiple curves is approximately equivalent to the result on a surface when the distance Δ_d between two adjacent curves is small enough.

For each sample circle C_i , a polynomial function f_i^g is obtained by fitting the information gain of all the discrete sample points $\mathbf{p}_{i,j}$ along C_i . The position of $\mathbf{p}_{i,j}$ is determined by $\theta_{i,j}$ from (10), and thus the gain $g_{i,j}$ relates the angle $\theta_{i,j}$ according to (12). Therefore, we define the continuous information gain function f_i^g as

$$f_i^g(\vartheta) = a_{i,0} + a_{i,1} \cdot \vartheta + a_{i,2} \cdot \vartheta^2 + \dots + a_{i,n} \cdot \vartheta^n \quad (13)$$

where ϑ , the domain of function f_i^g , denotes the continuous scanning angle variable along C_i , as shown in Fig.3; $\mathbf{A}_i := (a_{i,0}, a_{i,1}, \dots, a_{i,n})^T \in \mathbb{R}^{n+1}$ denotes the stacked weight parameters to be calculated, and n denotes the degree of the polynomial function.

The information gain values of all the sample points along C_i should fit the function (13). By stacking the relative sample points, we have

$$\mathbf{G}_i = \Theta_i \mathbf{A}_i, \quad (14)$$

where Θ_i denotes the Vandermonde matrix of $\theta_{i,j}, j \in (0, 1, 2, \dots, N_{SP})$, given as

$$\Theta_i := \begin{bmatrix} 1 & \theta_{i,0} & \theta_{i,0}^2 & \cdots & \theta_{i,0}^n \\ 1 & \theta_{i,1} & \theta_{i,1}^2 & \cdots & \theta_{i,1}^n \\ 1 & \theta_{i,2} & \theta_{i,2}^2 & \cdots & \theta_{i,2}^n \\ \vdots & \vdots & \vdots & \ddots & \vdots \\ 1 & \theta_{i,N_{SP}} & \theta_{i,N_{SP}}^2 & \cdots & \theta_{i,N_{SP}}^n \end{bmatrix}; \quad (15)$$

$\mathbf{G}_i := (g_{i,0}, g_{i,1}, \dots, g_{i,N_{SP}})^T$, which is calculated by (12).

The least squares method is utilized to solve \mathbf{A}_i , and we have

$$\mathbf{A}_i = (\Theta_i^T \Theta_i)^{-1} \Theta_i^T \mathbf{G}_i. \quad (16)$$

The solution of the weight parameters \mathbf{A}_i is analytical, contributing to computationally efficient. By fitting curves for each sample circle C_i , N_{AP} polynomial functions are obtained for representing the information gain about the local environment. Fig.4 illustrates the process of information curves fitting.

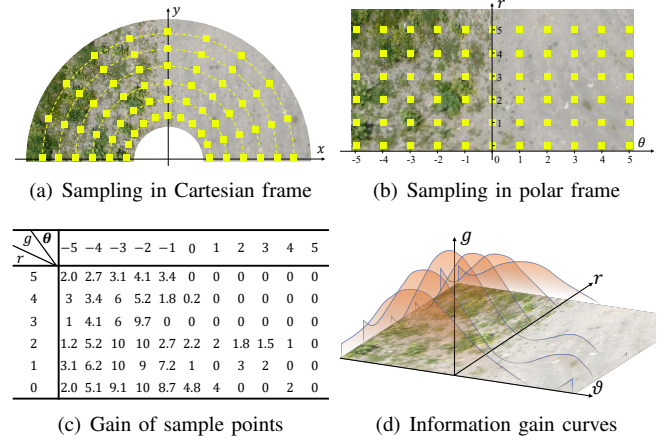


Fig. 4. Illustration of information gain curve fitting. (a) The yellow squares denote the sample points $\mathbf{p}_{i,j}$. The example environment includes feature-rich grass (left area) and featureless ground (right area). (b) The sample points are transferred into polar coordinates with θ and r as horizontal and vertical axes. The units of r and θ axes are m and rad , respectively. (c) The information gain of the sample points. (d) Each curve is fitted as a polynomial with degree $n=6$ from the sample points along corresponding sampling circle.

The best point ϑ_i^b with the maximal information gain of the single polynomial function f_i^g is obtained by

$$\vartheta_i^b = \arg \max_{\vartheta} f_i^g(\vartheta). \quad (17)$$

The solution of (17) is obtained with the gradient descent method. Note that $f_i^g(\vartheta)$ is a non-convex function, suffering from the local minimal problem. Fortunately, according to the processes in Sections IV-A and IV-B, the best sample point ${}^s\mathbf{p}_i^b$ is easily obtained by comparing all sample points along C_i . ${}^s\mathbf{p}_i^b$ provides a reliable initial value for numerical optimization of (17), where the ϑ value of ${}^s\mathbf{p}_i^b$ is obtained from (9). The best sample point ${}^s\mathbf{p}_i^b$ for C_i and the best point \mathbf{p}_i^b for f_i^g are demonstrated in Fig.3.

An information gain model F is formulated to obtain the global best point $\bar{\mathbf{p}}^b$ with in all polynomial functions about the local environment. The formulation is given as

$$F(\chi^{\text{wc}}, \mathcal{M}, \mathbf{p}) = \sum_{i=0}^{N_{AP}} \delta(\mathbf{p}) \cdot f_i^g(\vartheta) \quad (18)$$

where δ is a unit impulse function—the value of $\delta(\mathbf{p})$ is 1 if the point \mathbf{p} is at the i th sample circle C_i , otherwise $\delta(\mathbf{p})$ is 0.

The problem of obtaining the global best point $\bar{\mathbf{p}}^b$ with maximal information gain is formulated as

$$\bar{\mathbf{p}}^b := \arg \max_{\mathbf{p}} F(\chi^{\text{wc}}, \mathcal{M}, \mathbf{p}). \quad (19)$$

The optimization problem is solved by selecting the point with maximal information gain in $\{\mathbf{p}_0^b, \mathbf{p}_1^b, \dots, \mathbf{p}_i^b, \dots, \mathbf{p}_{N_{AP}}^b\}$ as the global best point $\bar{\mathbf{p}}^b$. The global best point is shown as the solid blue circle in Fig.3.

D. Receding Horizon Optimization

The optimal point $\tilde{\mathbf{p}}^b$ is obtained by evaluating the local environment information gain at the current robot state. This is also known as single-step optimization. However, the executed point sequence obtained by sequential single-step optimizations is discontinuous and disordered, resulting in unnecessary or uninformative motion. Because single-step optimization obtains the optimal point with only considering the current state and cannot involve future states to perform overall optimization for the future point sequence. Therefore, optimizing the point sequence in a horizontal sliding window is needed for robust and continuous motion planning of the camera. Then, a method based on the receding horizon optimization is developed to maximize the environmental information of future point sequence and minimize motion smoothness cost between neighbor points in the sequence.

Because the trajectory of robot base is a prior given, the future robotic positions in L steps, defined as $\{\chi_{k+1}^{wc}, \dots, \chi_{k+L}^{wc}\}$, are available from the trajectory. Note that even if the trajectory is unknown, the robot can predict the future positions by a constant velocity motion model. We assume that the voxel map \mathcal{M} maintains the same during the time of the horizontal sliding window. Then, the optimization problem including the information gain and motion smoothness is defined as

$$\tilde{\mathbf{p}}_{k+1:k+L}^b = \arg \min_{\tilde{\mathbf{p}}_{k+1:k+L}} -\lambda_{info} \mathcal{J}_{info} + \lambda_{smo} \mathcal{J}_{smo} \quad (20)$$

where $\tilde{\mathbf{p}}_{k+1:k+L}$ denotes the view-landing-points to be optimized in the horizontal sliding window; \mathcal{J}_{info} denotes the information gain; \mathcal{J}_{smo} denotes the smoothness cost penalizing trajectory discontinuity; λ_{info} and λ_{smo} are weight coefficients to balance the two terms \mathcal{J}_{info} and \mathcal{J}_{smo} - the more significant value of one coefficient than the other, the more concerned about the related term. The values of λ_{info} and \mathcal{J}_{smo} were set empirically. From (18), the information gain term \mathcal{J}_{info} is defined as

$$\mathcal{J}_{info} = \sum_{t=k+1}^{k+L} \left(\frac{1}{2} F(\chi_t^{wc}, \mathcal{M}, \tilde{\mathbf{p}}_t)^2 \right) \quad (21)$$

where $\tilde{\mathbf{p}}_t$ denotes the point to be optimized at time t . Further, to avoid unnecessary or discontinuous motion, the smoothness cost term \mathcal{J}_{smo} is given by evaluating the variation between neighbor points. The displacement vector between $\tilde{\mathbf{p}}_t$ and $\tilde{\mathbf{p}}_{t-1}$ is calculated as $\Delta \tilde{\mathbf{p}}_t = \tilde{\mathbf{p}}_t - \tilde{\mathbf{p}}_{t-1}$. And then, the smoothness cost term is defined as

$$\mathcal{J}_{smo} = \sum_{t=k+1}^{k+L} (\Delta \tilde{\mathbf{p}}_{t+1} - \Delta \tilde{\mathbf{p}}_t)^2, \quad (22)$$

this term constrains the neighbor displacement vectors in both the direction and length. The cost indicates the smoothness and distance distribution of $\tilde{\mathbf{p}}_{t+1}$, $\tilde{\mathbf{p}}_t$, and $\tilde{\mathbf{p}}_{t-1}$.

Since the complex information gain function in (12) is converted to the formulation in (18) which is differentiable, the optimization problem (20) is solved by using the gradient descent method [28]. And the single-step optimized point $\tilde{\mathbf{p}}_t^b$ by (19) is used as initial state. The $\tilde{\mathbf{p}}_t$ iterates as follows

$$\tilde{\mathbf{p}}_t := \tilde{\mathbf{p}}_t - \left(\lambda_{info} \cdot \frac{\partial \mathcal{J}_{info}}{\partial \tilde{\mathbf{p}}_t} + \lambda_{smo} \cdot \frac{\partial \mathcal{J}_{smo}}{\partial \tilde{\mathbf{p}}_t} \right). \quad (23)$$

The gradient of \mathcal{J}_{info} with respect to $\tilde{\mathbf{p}}_t$ is calculated as

$$\frac{\partial \mathcal{J}_{info}}{\partial \tilde{\mathbf{p}}_t} \Leftrightarrow \frac{\partial \mathcal{J}_{info}}{\partial \theta_t} \Leftrightarrow \frac{\partial f_i^g}{\partial \theta_t} = \sum_{s=1}^n a_{i,s} \cdot (\theta_{i,t})^{s-1} \quad (24)$$

where \Leftrightarrow denotes logical equivalence; the first \Leftrightarrow indicates that $\tilde{\mathbf{p}}_t$ and θ_t represent the same point; the second \Leftrightarrow indicates that only one polynomial function f_i^g in F relates to the variable $\tilde{\mathbf{p}}_t$ when $\delta(\tilde{\mathbf{p}}_t) = 1$ according to (18), because f_i^g is fitting from the sampling circle C_i where $\tilde{\mathbf{p}}_t$ lays in, and C_i is determined by the distance between $\tilde{\mathbf{p}}_t$ and χ_t^{wc} through (10). The gradient of \mathcal{J}_{smo} with respect to $\tilde{\mathbf{p}}_t$ is calculated as

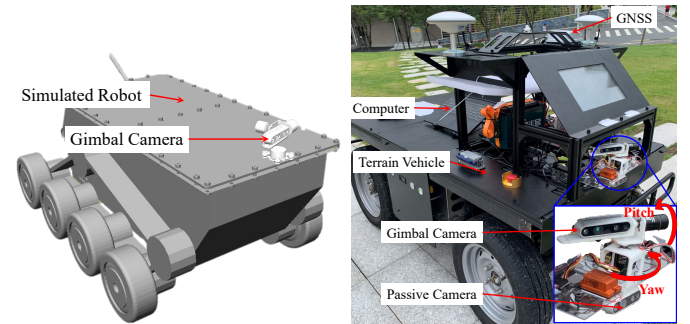
$$\frac{\partial \mathcal{J}_{smo}}{\partial \tilde{\mathbf{p}}_t} = -4 * (\tilde{\mathbf{p}}_{t+1} - 2 \cdot \tilde{\mathbf{p}}_t + \tilde{\mathbf{p}}_{t-1}). \quad (25)$$

For receding horizon optimization, the optimizing variable is the point sequence $\tilde{\mathbf{p}}_{k+1:k+L}$, where each point iterates according to (23). And the iteration step index of (23) is omitted for simplicity of statement. After iterating $\tilde{\mathbf{p}}_{k+1:k+L}$ until convergence, the optimal solution of the best point sequence is obtained and remarked as $\tilde{\mathbf{p}}_{k+1:k+L}^b$. The solution balanced information gain and motion smoothness in the horizontal time window. Finally, the first point $\tilde{\mathbf{p}}_{k+1}^b$ in $\tilde{\mathbf{p}}_{k+1:k+L}^b$ is selected as the next desired best point. The bottom tracking controller is then utilized to output control vector u^* according to the inverse kinematics and drive the gimbal camera towards $\tilde{\mathbf{p}}_{k+1}^b$.

Further, the view direction may swing with the robot base in practical field environments when moving on rough terrains. The gimbal's bottom controller is used not only to track the best point but also to improve the localization failure problem caused by the view direction swing by controlling the gimbal's pitch. Moreover, the controller outputs control commands at a high frequency with 100Hz.

V. SIMULATIONS AND EXPERIMENTS

A. Physical-engine simulation and experimental platforms



(a) Gazebo simulated robot (b) Experimental terrain vehicle
Fig. 5. Simulation and experiment platforms.

Several simulations and experiments were performed to verify the proposed approach. We built a mobile platform in the physics engine-based simulator Gazebo, and utilized an experimental terrain vehicle, as shown in Fig.5. An RGB-D camera on the gimbal was equipped for perception in the simulations and experiments. Another RGB-D camera was fixed on the robot to compare the passive method. The gimbal is of two-axis, with the pitch and yaw angles being controllable. A high-precision GNSS was used to provide ground truth in the experiments. The parameters are listed in

TABLE I. P_{min} was set $2m$, which can exclude the evaluation of the features too close to the camera.

TABLE I
EXPERIMENT PARAMETERS

Camera FOV	$69^\circ \times 42^\circ$	Δ_d	0.4 m	n	6
Camera resolution	640×480	Δ_θ	20°	L	6
Max. sensor range	10 m	P_{min}	2 m	λ_{info}	1
Max. velocity	20 km/h	N_{AP}	10	λ_{smo}	0.12
Voxel size	0.4 m	N_{SP}	18		

B. Evaluation of information mapping method

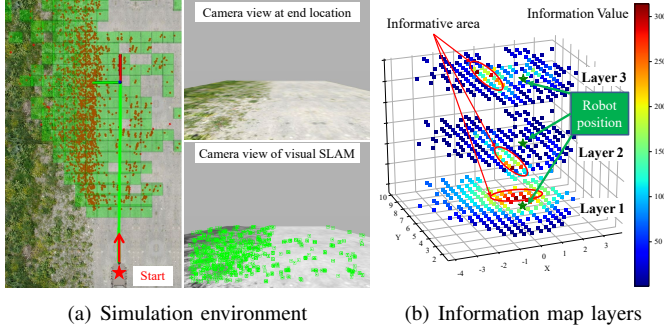


Fig. 6. Illustration of information mapping. (a) The red dots denote the built map points, the green line denotes the robotic trajectory, and the green voxels denote the voxel map made from the map points. (b) Layer 1, Layer 2, and Layer 3 denote the maps for calculating Fisher information, feature distribution information and weighted Fisher information, respectively. The heat map represents the information value at each voxel.

We first performed a simulation to evaluate the proposed information mapping method. Figure 6(a) illustrates the top view of an example environment. The robot's left side is texture-rich grass, and the right side is textureless ground. The robot with the fixed camera traveled along the trajectory shown as the green line in Fig.6(a). As shown in Fig.6(b), the information maps are built by different information formulations, i.e., the Fisher information in (5), the feature distribution information in (8), and the distribution-weighted Fisher information map (Layer 3) complements the Fisher information with the feature distribution information. It is seen that the information representation provided in Layer 3 is more accurate compared to the other two methods, because the area takes both the Fisher information and the feature distribution information into consideration according to (9).

Since the Fisher information in the above simulations considered the uncertainty of the voxel position by the covariance \mathbf{Q} , we additionally performed simulations to verify the effects of feature uncertainty on the information mapping method. The feature uncertainty is represented by $\mathbf{Q}^* = \text{diag}(\delta_p^2, \delta_p^2, \delta_z^2)$ where $\delta_p^2 = 0.25$ denotes the feature

points' pixel error and $\delta_z = 1.425 \times 10^{-6} z^2 (mm^2)$ depends on depth measurement [29]. The results show that the information distribution with and without adding feature uncertainty \mathbf{Q}^* are consistent. In addition, the detection stability of 2D feature points can be one source of feature uncertainty. According to our tests, the whole feature point map output from SLAM can distinguish feature distribution differences well and guide for view planning, even though the detected 2D features are not exactly the same in each operation even in the same environment. Therefore, the feature uncertainty has minor effects on the information distribution and does not affect the active view planning for perception in this work.

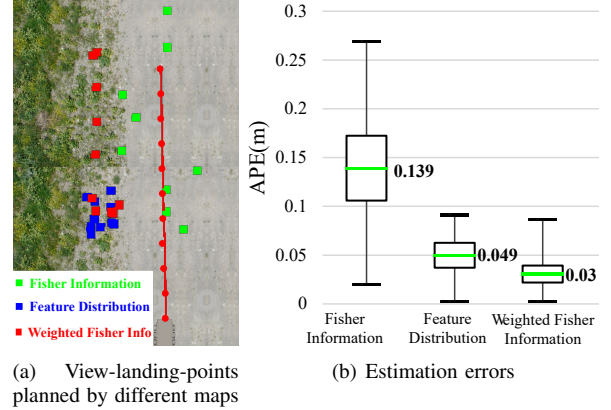


Fig. 7. Evaluation Simulation results of localization accuracy under different information mapping methods. (a) The red line denotes the robotic trajectory, the red dots denote the trajectory points at different timestamps. The colored squares represent the best view-landing-points under different information maps. (b) The mean APE is denoted by a green line, while the STD of the estimation error is denoted by a black box.

To evaluate the performance of different information mapping methods on the localization accuracy, we designed a simulation to make the robot travel 6 meters along a straight line. Without loss of generality, we utilized the regular sampling method in Section IV.A to plan the camera view (i.e., view-landing-point). The planned view-landing-points were illustrated in Fig.7(a) under different information maps. The absolute pose error (APE) between the estimated trajectory and the ground truth trajectory [30] is used to quantify localization accuracy after repeating the simulation five times, as shown in Fig.7(b). It is seen that the Fisher information map exhibited maximum estimation error because the planned view-landing-points (the green squares in Fig.7(a)) scattered on the textureless ground. Indicated by blue squares in Fig.7(a), the view-landing-points planned under the feature distribution information map concentrated on the known area that has been visited, thus exhibiting smaller tracking errors than the Fisher information map. However, using only the feature distribution information map leads to exploration degeneration, and makes the camera towards to the back of the robot and to be unfavorable for feature tracking in this work. Indicated by the red squares in Fig.7(a), the view-landing-points of the distribution-weighted Fisher information map laid on the texture-rich grass. Hence, the estimation error performed well with the smallest error. Moreover, compared with the feature distribution information map, the distribution-weighted Fisher information map made the view-landing-points be distributed

at the upper right of the robot pose. Because the points closer to the robot have higher Fisher information according to the definition in (4), which makes the fusion of Fisher information and the distribution information alleviate the degree of exploration degeneration. Therefore, the distribution-weighted Fisher information map is more suitable for view planning thanks to considering both the quality and distribution of the environmental features.

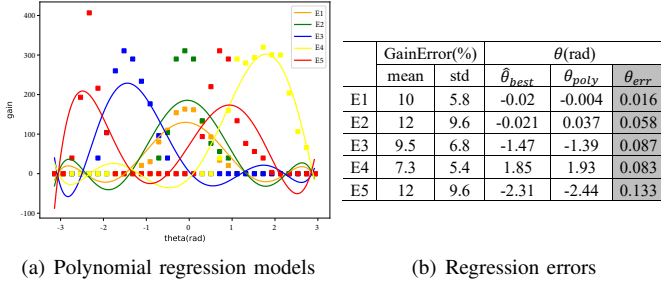


Fig. 8. Evaluation of the polynomial regression accuracy.

We have collected data at representative locations (i.e., E1, E2, E3, E4, and E5) to evaluate the accuracy of polynomial regression. Each of the obtained regression models indicated by coloured curves in Fig.8(a) is based on the points sampled along a circle around the robot location with the interval angle $\Delta\theta = 0.2rad$. The information gain at each sample point is calculated by (12) and indicated by a coloured small square. In Fig.8(b), the second and third columns denote the gain error between the ground truth gain and the polynomial regression gain of the sampled points, respectively. Moreover, our work concentrates on the accuracy of the angle θ rather than the information gain because the planner finally uses the angle θ with the maximum information gain as the best view direction. The angle error θ_{err} between $\hat{\theta}_{best}$ and θ_{poly} is used to measure the regression accuracy. $\hat{\theta}_{best}$ denotes the true angle with maximum information gain, and the angle is obtained by dense sampling with the interval $\Delta\theta = 0.01rad$. θ_{poly} denotes the maximum information angle obtained from the regression polynomial by the global optimization. From Fig.8(b), the θ_{err} of the polynomial curves regressed on data of E1, E2, E3, E4, and E5 are with a small value below $0.133 rad$. From Fig.8(a), it is noted that the optimal angle obtained from the polynomial regression still stays near the area with high information, even though there exists regression error. This makes the localization accuracy improved by looking to the informative area. Furthermore, according to our tests on the regression speed and accuracy performance, the time cost decreases and the error increase when the sample interval grew.

C. Evaluation of camera view planning algorithm

The proposed camera view planning approach for robust visual SLAM includes information mapping and camera view planner IGLOV. The information mapping module has been verified in the previous section; therefore, we further designed several simulations to evaluate the performance of IGLOV planner. We compared the proposed IGLOV planner with several existing planning methods, including the passive method (PAS), uniform sampling in view space (USV) [31], Monte

Carlo sampling in task space (MST) [32], regular sampling considering degeneration in task space (RSDT). For fair comparison, the previous weighted-Fisher information mapping method was used for these camera view planning approaches. PAS method fixed the camera on the robot base and did not change the viewing direction. USV method sampled ten views uniformly in $[-\pi, \pi]$ of yaw at each timestamp and evaluated each view to find the maximal information view. MST method, also called random sampling method in [32], sampled 500 points around the robot within 5m at each timestamp and evaluated each point to find the one with maximal information. USV and MST evaluate the information according to (9). RSDT method sampled points according to (10) and selected the sample point with maximal information gain as the best view-landing-point according to (12). RSDT considered the consistency between the view and the motion direction but without applying the polynomial regression and receding horizon optimization.

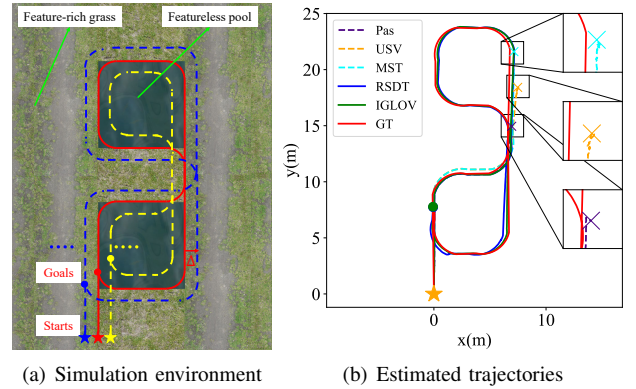


Fig. 9. Simulation 1 and the results under different methods. (a) Two featureless pools lie in a grass plane, and the trajectories with different colors represent various offsets from the baseline trajectory. (b) Estimated trajectories under different planning methods at offset $\Delta = -0.6$. GT is the ground truth indicated by the solid red trajectory. The orange star marker is the start point of the trajectories. The circular markers ‘•’ with different colors represent the endpoint of a successful tracking, while the ‘×’ markers represent the endpoint of a failed tracking.

The first scene simulated a wild environment, as shown in Fig.9(a). The red curve denotes a preplanned baseline trajectory of the robot; the blue and yellow dot curves are obtained by transforming the baseline trajectory with a positive offset $\Delta > 0$ and negative offset $\Delta < 0$, respectively. Positive offset zooms the trajectory to the feature-rich area, while negative offset shrinks the trajectory to the featureless area. The simulated robot moved along five trajectories with $\Delta = \{0.6, 0.3, 0, -0.3, -0.6\}$ meters. The simulation also investigated how the proportion of featureless areas affects localization accuracy.

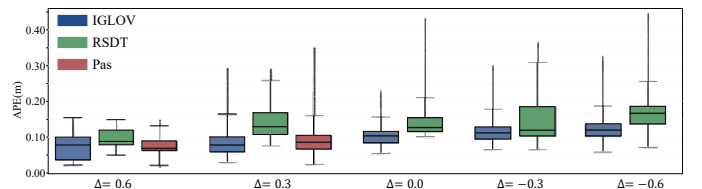


Fig. 10. Estimation errors under different planning methods with various offsets Δ . The results of USV and MST are not presented due to the estimation failures.

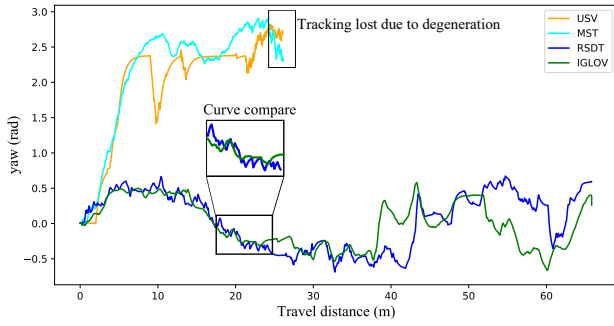


Fig. 11. Gimbal's yaw angle curve versus travel distance at the simulation with $\Delta = -0.6$.

As shown in Fig.10, the PAS method localized well with positive Δ thanks to the high proportion of featurerich areas in FOV. The USV and MST failed to localize the robot in all simulations. The gimbal's yaw angle curves for the simulation with $\Delta = -0.6$ in Fig.11 demonstrated the reason of localization failure. The yaw angles in orange and cyan curve reach a high value about 3.0rad after traveled 23m, which means the gimbal camera looked towards the robot's back by using the USV and MST methods; this resulted in the exploration degeneration and loss of feature tracking. The details can be shown in the attached video. In addition, the trajectories under the different methods at $\Delta = -0.6$ are shown in Fig.9(b). From Fig.10, the RSDT's performance degraded when Δ decreased. Because RSDT does not consider the receding horizon optimization especially the motion smoothness cost, resulting in shaking rotations. The proportion of featureless areas in the image increased when Δ decreased, and this made the shaking rotation of planned camera view influence the localization accuracy more obviously. Fig.11 shows that the yaw angle of the RSDT method changed with high-frequency ripples and brought sudden motions of the gimbal camera, degrading the feature matching and tracking of the SLAM. Thanks to the consideration of degeneration and motion smoothness in the horizontal time window, the IGLOV planner performed much more smoothly, and the camera views were almost consistent with the motion direction because the yaw angles were smaller than 0.5 rad. Moreover, the views also turned to the feature-rich regions by the informative planning, this makes the camera by IGLOV locate well with the smallest estimation error, as shown in Fig.10.

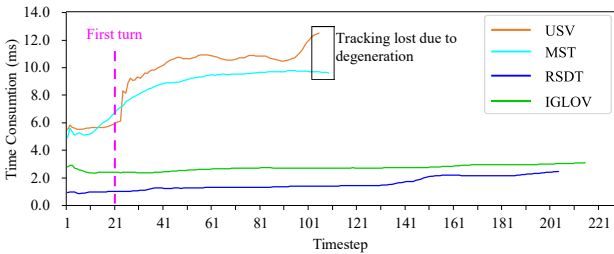


Fig. 12. Computation costs of different methods in one planning period.

The computation costs of different methods are compared in Fig.12. The time costs of the USV and MST methods positively correlate with the map size; the sudden increase of computation time occurred at the first turn of the trajectory because many new map points were added to the maps. While the RSDT and IGLOV methods cost less time because the

regular sampling method brings less sampling and evaluation. Besides, the IGLOV planner takes more time than the RSDT method due to the polynomial fitting and optimization.

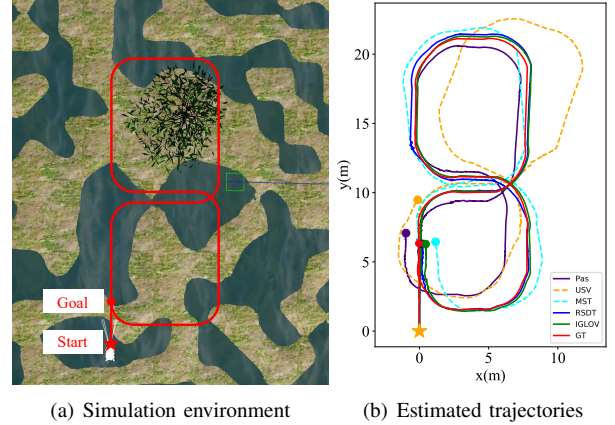


Fig. 13. Simulation 2 and estimated trajectories under different methods. (a) Several featureless puddles lay in a rough grass plane, and a tree lays in the environment center. The robot was required to travel along the red trajectory. (b) Estimated trajectories under different methods. (c) Localization accuracy of different methods.

TABLE II
LOCALIZATION ACCURACY OF SIMULATION 2.

	Pas	USV	MST	RSDT	IGLOV
Mean(m)	0.783	1.036	0.343	0.194	0.139
RMSE(m)	0.954	1.234	0.413	0.219	0.167

We further designed another simulation in a common wild environment, as shown in Fig.13(a). The estimated trajectories, as well as the ground truth, are shown in Fig.13(b). The PAS method exhibited large errors because the featureless water surface occupied the camera FOV in some parts of the trajectory. Although the view-landing-points under the MST and USV methods lay on the feature-rich regions, most of them lead the camera view opposed the motion direction; therefore, the two methods exhibited large errors due to the degeneration problem. In contrast, the RSDT and IGLOV methods performed well in this environment. TABLE II shows that the IGLOV planner has the minimal localization error than other methods because the estimation uncertainty, exploration and motion smoothness are considered.

D. Experiments

Further, we designed several real-world experiments to verify the proposed approach with the experimental ground vehicle shown in Fig.5(b). Because both the USV and MST methods led to SLAM failures in our experiments, we only presented the comparison between the passive method and the proposed one. We performed the first experiment in a typical outdoor campus environment with the robot moving along the campus road, while the second experiment was performed on a hillside with rough grass terrain.

1) *Experiment 1*: The first experiment (Ex1) was performed along a trajectory about 500m in Shenzhen University Town, as shown in Fig.14. The estimation error under the two methods are shown in TABLE III. The IGLOV method performed better in mean and RMSE values. Compared to the simulation results in Section V.C, the localization accuracy of

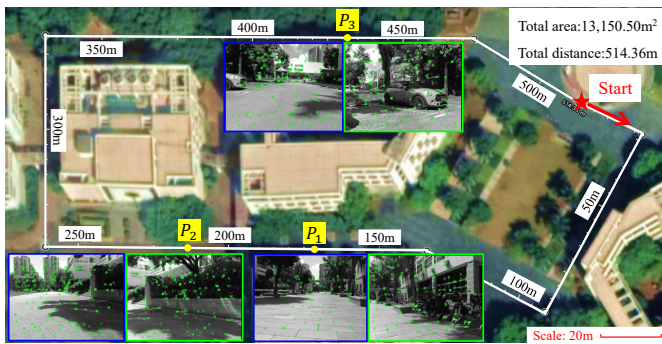


Fig. 14. Bird's-eye view of the environment and the required trajectory in Experiment 1. The white line denotes the required trajectories. P_1 - P_3 are the positions selected to show typical planning results. The subfigures with blue and green boxes are captured by the passive camera and the gimbal camera with IGLOV methods, respectively.

TABLE III
LOCALIZATION ACCURACY OF EXPERIMENTS.

		Max(m)	Mean(m)	Min(m)	RMSE(m)
Ex1	Pas	2.552	0.892	0.041	1.027
	IGLOV	2.212	0.839	0.369	0.901
Ex2	Pas	2.289	1.242	0.341	1.322
	IGLOV	1.718	0.734	0.152	0.814

the passive method in the experiment was much closer to the IGLOV method. The reason is that the operating environment is urbanized and surrounded by feature-rich parterres, trees, and buildings; thus, the passive method also tracked well with sufficient features in each keyframe. However, when traveling along the trajectory, the IGLOV planner evaluated the information of the local environments and autonomously turned the camera view towards the areas with maximum information gain. Some typical planning results are demonstrated as the subfigures in Fig.14. The IGLOV method always turned the camera towards the local feature-rich areas, like the parked bicycles at position P_1 , the high parterre at position P_2 , and the parked car at position P_3 . Although the improvement of localization accuracy was limited in the urbanized environments, the proposed method efficiently guided the camera view to local feature-rich areas.

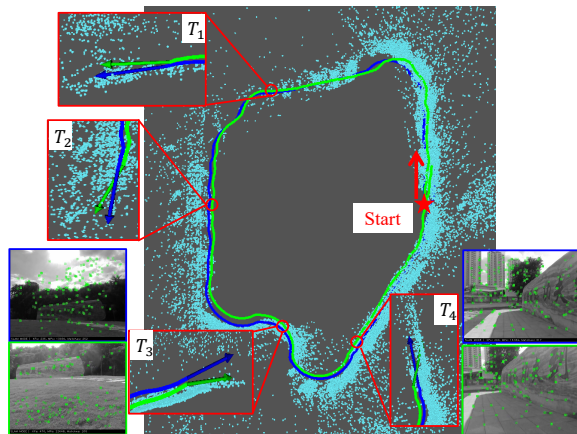


Fig. 15. Typical planning results of T_1 - T_4 in Experiment 2. The blue and green arrows in the subfigures denote the directions of the passive camera and the gimbal camera by IGLOV methods, respectively. The images with blue and green boxes are captured by the passive camera and the gimbal camera with IGLOV methods, respectively.

2) *Experiment 2*: We further designed an experiment (Ex2) in a wild terrain environment to evaluate the performance of the proposed approach. As shown in Fig.1, the experiment was performed on a hillside, the trajectory length was about 130m. The trajectory estimation results under the passive and the IGLOV methods, together with the ground truth, are shown in Fig.1. It is seen that the estimated trajectory under the IGLOV planner (green line) is closer to the ground truth (red line) than that under the passive method (blue line). The proposed approach is designed based on task space and feature points in the local sampling range; this makes the gimbal camera pay more attention to the feature-rich areas once it appears in the sampling range and then decreases the localization error. TABLE III shows the results for quantitative analysis. The visual SLAM was run without loop closure. The IGLOV planner performed much better than the passive method; the reason is that the camera avoided the view to the featureless areas like the sky or the pavement and focused on local feature-rich areas like the steles or the trees.

The gimbal camera actively changed the view direction to the feature-rich regions shown as the subfigures in Fig.15. Our approach stabilized the view direction towards the slope to complement the view direction swing in rough terrains at location T_3 ; this avoided the glare caused by direct sunlight irradiation. In contrast, the sky occupied a large part of the camera FOV under the passive method. With the help of the IGLOV method, the gimbal camera looked towards the feature-rich stele for helpful information at location T_4 .

VI. CONCLUSION

The paper develops a novel approach to realize active visual SLAM for ground or surface robots in challenging outdoor environments. An information mapping algorithm is first proposed to represent the environmental information richness efficiently; the algorithm makes the online active view-planning possible. A continuous information modeling method combined the regular sampling and polynomial regression is proposed to map the environmental information around the robot into multiple polynomial functions. Based on the multiple polynomial functions, the informative planning problem is solved efficiently by numerical optimization. A receding horizon optimization-based method solves the view planning problem under degeneration and motion smoothness constraints. Finally, several physical-engine simulations and experiments in outdoor environments are performed. The comparisons to the existing state-of-the-art approaches have verified the effectiveness of the proposed approach. Our future work will focus on integrating robotic trajectory planning into the active SLAM for autonomous environmental exploration and informative navigation by considering map uncertainty, estimation of motion noise, infrared distribution and traversability simultaneously. We will also study the robustness of vSLAM with the severe and high-frequency oscillations due to fast movement on rough terrains.

REFERENCES

- [1] R. Duan, D. P. Paudel, C. Fu, and P. Lu, "Stereo orientation prior for uav robust and accurate visual odometry," *IEEE/ASME Transactions on Mechatronics*, vol. 27, no. 5, pp. 3440–3450, 2022.

- [2] J. Liu, X. Li, Y. Liu, and H. Chen, "Rgb-d inertial odometry for a resource-restricted robot in dynamic environments," *IEEE Robotics and Automation Letters*, vol. 7, no. 4, pp. 9573–9580, 2022.
- [3] R. Mur-Artal and J. D. Tardós, "ORB-SLAM2: an open-source SLAM system for monocular, stereo and RGB-D cameras," *IEEE Transactions on Robotics*, vol. 33, no. 5, pp. 1255–1262, 2017.
- [4] T. Qin, P. Li, and S. Shen, "Vins-mono: A robust and versatile monocular visual-inertial state estimator," *IEEE Transactions on Robotics*, vol. 34, no. 4, pp. 1004–1020, 2018.
- [5] Z. Wang, J. Zhang, S. Chen, C. Yuan, J. Zhang, and J. Zhang, "Robust high accuracy visual-inertial-laser slam system," in *2019 IEEE/RSJ International Conference on Intelligent Robots and Systems (IROS)*. IEEE, 2019, pp. 6636–6641.
- [6] H. Matsuki, L. Von Stumberg, V. Usenko, J. Stückler, and D. Cremers, "Omnidirectional dso: Direct sparse odometry with fisheye cameras," *IEEE Robotics and Automation Letters*, vol. 3, no. 4, pp. 3693–3700, 2018.
- [7] Z. Zhang, H. Rebecq, C. Forster, and D. Scaramuzza, "Benefit of large field-of-view cameras for visual odometry," in *2016 IEEE International Conference on Robotics and Automation (ICRA)*. IEEE, 2016, pp. 801–808.
- [8] S. Frintrop and P. Jensfelt, "Attentional landmarks and active gaze control for visual slam," *IEEE Transactions on Robotics*, vol. 24, no. 5, pp. 1054–1065, 2008.
- [9] Y. Chen, S. Huang, and R. Fitch, "Active slam for mobile robots with area coverage and obstacle avoidance," *IEEE/ASME Transactions on Mechatronics*, vol. 25, no. 3, pp. 1182–1192, 2020.
- [10] Y. Wang, H. Chen, S. Zhang, and W. Lu, "Automated camera-exposure control for robust localization in varying illumination environments," *Autonomous Robots*, vol. 46, no. 4, pp. 515–534, 2022.
- [11] X. Deng, Z. Zhang, A. Sintov, J. Huang, and T. Bretl, "Feature-constrained active visual slam for mobile robot navigation," in *2018 IEEE International Conference on Robotics and Automation (ICRA)*. IEEE, 2018, pp. 7233–7238.
- [12] K. Khosoussi, M. Giamou, G. S. Sukhatme, S. Huang, G. Dissanayake, and J. P. How, "Reliable graphs for slam," *The International Journal of Robotics Research*, vol. 38, no. 2-3, pp. 260–298, 2019.
- [13] Z. Zhang and D. Scaramuzza, "Fisher Information Field: an Efficient and Differentiable Map for Perception-aware Planning," *arXiv e-prints*, p. arXiv:2008.03324, Aug. 2020.
- [14] A. Hornung, K. M. Wurm, M. Bennewitz, C. Stachniss, and W. Burgard, "Octomap: An efficient probabilistic 3d mapping framework based on octrees," *Autonomous robots*, vol. 34, no. 3, pp. 189–206, 2013.
- [15] M. G. Jadidi, J. V. Miro, and G. Dissanayake, "Gaussian processes autonomous mapping and exploration for range-sensing mobile robots," *Autonomous Robots*, vol. 42, no. 2, pp. 273–290, 2018.
- [16] Z. Zhang and D. Scaramuzza, "Perception-aware receding horizon navigation for mavs," in *2018 IEEE International Conference on Robotics and Automation (ICRA)*. IEEE, 2018, pp. 2534–2541.
- [17] J. Strader, K. Otsu, and A.-a. Agha-mohammadi, "Perception-aware autonomous mast motion planning for planetary exploration rovers," *Journal of Field Robotics*, vol. 37, no. 5, pp. 812–829, 2020.
- [18] A. Kim and R. M. Eustice, "Active visual slam for robotic area coverage: Theory and experiment," *The International Journal of Robotics Research*, vol. 34, no. 4-5, pp. 457–475, 2015.
- [19] B. Zhou, Y. Zhang, X. Chen, and S. Shen, "Fuel: Fast uav exploration using incremental frontier structure and hierarchical planning," *IEEE Robotics and Automation Letters*, vol. 6, no. 2, pp. 779–786, 2021.
- [20] M. Dharmadhikari, T. Dang, L. Solanka, J. Loje, H. Nguyen, N. Khedekar, and K. Alexis, "Motion primitives-based path planning for fast and agile exploration using aerial robots," in *2020 IEEE International Conference on Robotics and Automation (ICRA)*. IEEE, 2020, pp. 179–185.
- [21] H. Zhu, J. J. Chung, N. R. Lawrance, R. Siegwart, and J. Alonso-Mora, "Online informative path planning for active information gathering of a 3d surface," in *2021 IEEE International Conference on Robotics and Automation (ICRA)*. IEEE, 2021, pp. 1488–1494.
- [22] V. Indelman, L. Carlone, and F. Dellaert, "Planning in the continuous domain: A generalized belief space approach for autonomous navigation in unknown environments," *The International Journal of Robotics Research*, vol. 34, no. 7, pp. 849–882, 2015.
- [23] T. D. Barfoot, *State estimation for robotics*. Cambridge University Press, 2017.
- [24] Y. Chen, L. Zhao, Y. Zhang, S. Huang, and G. Dissanayake, "Anchor selection for slam based on graph topology and submodular optimization," *IEEE Transactions on Robotics*, vol. 38, no. 1, pp. 329–350, 2021.
- [25] Z. Zhang and D. Scaramuzza, "Beyond point clouds: Fisher information field for active visual localization," in *2019 International Conference on Robotics and Automation (ICRA)*. IEEE, 2019, pp. 5986–5992.
- [26] A. N. Bishop, B. Fidan, B. D. Anderson, K. Doğançay, and P. N. Pathirana, "Optimality analysis of sensor-target localization geometries," *Automatica*, vol. 46, no. 3, pp. 479–492, 2010.
- [27] F. Pukelsheim, *Optimal design of experiments*. SIAM, 2006.
- [28] S. Boyd, S. P. Boyd, and L. Vandenberghe, *Convex optimization*. Cambridge university press, 2004.
- [29] P. F. Proenca and Y. Gao, "Probabilistic rgb-d odometry based on points, lines and planes under depth uncertainty," *Robotics and Autonomous Systems*, vol. 104, pp. 25–39, 2018.
- [30] M. Grupp, "evo: Python package for the evaluation of odometry and slam," *url: https://github.com/MichaelGrupp/evo*, 2017.
- [31] R. Zeng, W. Zhao, and Y.-J. Liu, "Pc-nbv: A point cloud based deep network for efficient next best view planning," in *2020 IEEE/RSJ International Conference on Intelligent Robots and Systems (IROS)*. IEEE, 2020, pp. 7050–7057.
- [32] N. Palomeras, N. Hurtós, M. Carreras, and P. Ridao, "Autonomous mapping of underwater 3-d structures: From view planning to execution," *IEEE Robotics and Automation Letters*, vol. 3, no. 3, pp. 1965–1971, 2018.



Zhihao Wang received the B.Eng. degree in mechanical engineering from the WuHan University of Technology, WuHan, China, in 2017, and the M.Eng. degree in control engineering from the Huazhong University of Science and Technology, WuHan, China, in 2019. He is currently working toward the Ph.D. degree in robotics with the School of Mechatronics Engineering and Automation, Harbin Institute of Technology, Shenzhen, China.

His research interests lie in robotic motion planning and control, 3D exploration and reconstruction.



Haoyao Chen received the B.Eng. degree in mechatronics and automation from the University of Science and Technology of China, Hefei, China, in 2004, and the Ph.D. degree in robotics and automation from the University of Science and Technology of China and the City University of Hong Kong, Hong Kong, in 2009.

He is currently a Professor with the Harbin Institute of Technology Shenzhen, Shenzhen, China, and the State Key Laboratory of Robotics and System, Harbin, China. His research interests lie in visual

servoing, multirobot systems, motion control, and aerial manipulation.



Shiwu Zhang (Member, IEEE) received the B.S. degree in mechanical and electrical engineering and the Ph.D. degree in precision instrumentation and precision machinery from the University of Science and Technology of China (USTC), Hefei, China, in 1997 and 2003, respectively.

He is currently a Professor with the Department of Precision Machinery and Precision Instrumentation, USTC. He is the author of more than 100 papers in different journals and conferences. His research interests include smart materials and their applications

in bio-inspired robots, amphibious robot, soft robots, and terradynamics.



Yunjiang Lou (Senior Member, IEEE) received the B.S. and M.E. degrees in automation from the University of Science and Technology of China, Hefei, China, in 1997 and 2000, respectively, and the Ph.D. degree in electrical and electronic engineering from the Hong Kong University of Science and Technology, Hong Kong, in 2006.

He is currently with the State Key Laboratory of Robotics and Systems and the Shenzhen Key Laboratory for Advanced Motion Control and Modern Automation Equipments, School of Mechatronics Engineering and Automation, Harbin Institute of Technology (Shenzhen), Shenzhen, China. His research interests include motion control, mechanism design, compliant actuators, and industrial robots.